Med Biol Eng Comput (2016) 54:1921–1933
DOI 10.1007/s11517-016-1486-9

ORIGINAL ARTICLE

Do the deceleration/acceleration capacities of heart rate reflect cardiac sympathetic or vagal activity? A model study

Qing Pan[1] · Gongzhan Zhou[1] · Ruofan Wang[2] · Guolong Cai[3] · Jing Yan[3] · Luping Fang[1] · Gangmin Ning[2]

Received: 5 August 2015 / Accepted: 4 March 2016 / Published online: 8 April 2016

Abstract Despite increased application of the deceleration capacity (DC) and acceleration capacity (AC) of heart rate indices as indicators of autonomic nervous system (ANS) function, it remains controversial as to whether they reflect cardiac sympathetic or vagal activity. We addressed this problem using a cardiovascular system model that allows analysis of DC and AC under controllable levels of sympathetic and vagal activities. Multi-scale DCs and ACs with various timescales T and wavelet scales s were computed from the simulated RR interval series under randomly fluctuating levels of ANS activity, and the correlations of the indices to ANS functions were assessed. Results showed that under the conventional scales ($T = 1$, $s = 2$), both DC and AC were solely dependent on vagal activity. With higher scales ($T = 3$, $s = 5$), both DC and AC were positively correlated to sympathetic activity and negatively correlated to vagal activity. These data suggest that DC and AC provide information on the same aspects of ANS activity and that their physiological significance is highly influenced by the timescales and wavelet scales used in the computation.

Keywords Deceleration capacity · Acceleration capacity · Autonomic nervous system · Mathematical model

1 Introduction

Imbalances in the autonomic nervous system (ANS) are frequently observed in cardiovascular diseases (CVDs), including hypertension, chronic heart failure (CHF), and myocardial infarction (MI) [13, 14, 26, 45]. Heart rate variability (HRV) is a noninvasive tool to quantitatively estimate cardiac autonomic imbalances [9, 18, 21]. Reduced HRV is a strong predictor of mortality after MI [37] and is associated with a series of other outcomes including CHF, hypertension, and diabetes mellitus [29, 35, 36, 42]. HRV is influenced by sympathetic and vagal modulation of the heart rate. However, the physiological basis of HRV remains unresolved [7, 23, 40]. In addition, some HRV measures can be confounded by external and internal perturbations, such as ectopic beats and errors in beat detection [24]. Development of more robust noninvasive measures of heart rate modulations with clear physiological interpretations is required to overcome these limitations.

Recently, a pair of novel indices, termed deceleration capacity (DC) and acceleration capacity (AC) of heart rate, was proposed to measure the deceleration- and acceleration-related HRV [5]. DC and AC are computed by applying a phase-rectified signal averaging (PRSA) algorithm to the RR interval (RRI) series. The PRSA method selects the decelerating and accelerating RRIs as the anchor points for DC and AC calculations, respectively. The sections around the anchor points are aligned and averaged to generate the PRSA average series. DC and AC are then computed as the coefficient of a Haar wavelet at scale two in the center

✉ Gangmin Ning
gmning@zju.edu.cn

[1] College of Information Engineering, Zhejiang University of Technology, 288 Liuhe Road, Hangzhou 310023, China

[2] Department of Biomedical Engineering, Key Laboratory of Biomedical Engineering of Ministry of Education, Zhejiang University, 38 Zheda Road, Hangzhou 310027, China

[3] Department of ICU, Zhejiang Hospital, 12 Lingyin Road, Hangzhou 310013, China

of the PRSA average series. The indices have shown high clinical significance, with DC verified to be superior to the conventional HRV index in predicting mortality after MI [4, 5, 19], while both DC and AC are effective biomarkers for CHF [32].

DC and AC attempt to separately assess sympathetic and vagal modulation through the measurement of deceleration- and acceleration-related HRV [5]. However, despite the increased application of DC and AC in the clinical setting, it remains controversial as to whether the indices reflect cardiac sympathetic or vagal modulation [3, 5, 8, 16, 32]. Some studies reported that DC reflects vagal activity and AC reflects sympathetic activity and that the criterion of anchor point selection in the PRSA method determines the physiological background of the indices. For example, Bauer et al. [5] suggested that DC reflects vagal activity, as heart rate deceleration is evoked by vagal stimulation. It therefore follows that AC reflects sympathetic function, as recently reported [3]. Kantelhardt et al. [17] also suggested that DC and AC could separately measure sympathetic and vagal functions based on the marked differences in the performances of DC and AC in predicting mortality after MI.

By contrast, DC and AC have also been suggested to reflect the same aspects of ANS activity and that the scales used in the computation of the indices are associated with their physiological interpretation. Campana et al. [8] reported that both DC and AC are modulated by vagal function, as they both measure the change in heart rate over a short timescale; similar correlations to aging were also found in healthy subjects. In a multi-scale DC and AC analysis [19], Kisohara et al. found that the predictive abilities of DC and AC computed with a scale higher than the conventional setting were independent of the conventional indices, suggesting that the scales used in the computation of DC and AC have an influence on their physiological interpretation.

We intended to use a cardiovascular system model to address these controversies. The model was developed by Ursino and Magosso [43, 44]. It is able to simulate realistic RRI series and analyze the respective roles of sympathetic and vagal activities in HRV, such as the low-frequency (LF) and high-frequency (HF) components in the power spectrum of the RRI series. Because DC and AC are generally regarded as variants of HRV [22], a model that is able to simulate HRV properties was adopted in this study. Based on this model, we tested whether the physiological interpretation of the indices was dependent upon the criterion of anchor point selection. For this purpose, the simulations were performed with randomly fluctuating sympathetic and vagal activities, and the correlations of DC and AC with ANS function were evaluated. We also examined whether the timescales and wavelet scales in the calculation of DC and AC influenced their correlation with ANS functions by computing multi-scale DCs and ACs and performing the correlation analysis.

2 Methods

2.1 Model description and parameterization

The model developed by Ursino and Magosso [43, 44] consists of two parts. One part is a hemodynamic model, which includes the four chambers of the heart, six systemic vascular compartments, and three pulmonary vascular compartments. Each compartment was described by an electrical circuit with a resistance, a capacitance, and an inductance. These compartments are connected to form a closed-loop cardiovascular system model, in which the time-dependent blood pressure and flow rate can be simulated. The other part is an ANS regulating model, which adjusts the peripheral resistance, the venous unstressed volume, and the heart period in response to the stimuli from the carotid baroreceptor (CBR) and the lung stretch receptor (LSR). Details of the model have been previously reported [43, 44]. As heart rate variation was the most important output in the present study, the model of heart rate regulation is described in detail below.

A diagram of the model of heart rate regulation and its connection to the hemodynamic model are shown in Fig. 1. Heart period is modulated by the co-activation of the sympathetic and vagal limbs via their responses to stimuli from the CBR and the LSR. The governing equations hold as

$$v_T = G_{aTv} \cdot (P_{sa} - P_{san}) - G_{pTv} \cdot (V_L - V_{Ln}) \tag{1}$$

$$s_T = G_{aTs} \cdot (P_{sa} - P_{san}) + G_{pTs} \cdot (V_L - V_{Ln}) \tag{2}$$

$$\frac{\mathrm{d}x_{Tv}(t)}{\mathrm{d}t} = \frac{1}{\tau_{Tv}} \cdot [v_T(t - D_{Tv}) - x_{Tv}(t)] \tag{3}$$

$$\frac{\mathrm{d}x_{Ts}(t)}{\mathrm{d}t} = \frac{1}{\tau_{Ts}} \cdot [s_T(t - D_{Ts}) - x_{Ts}(t)] \tag{4}$$

$$x_T = x_{Tv} + x_{Ts} \tag{5}$$

$$k_T = \left(\mathrm{RR_{max}} - \mathrm{RR_{min}}\right)/(4 \cdot S_{\mathrm{T0}}) \tag{6}$$

$$\mathrm{RR} = \frac{\mathrm{RR_{min}} + \mathrm{RR_{max}} \cdot \mathrm{e}^{x_T/k_T}}{1 + \mathrm{e}^{x_T/k_T}} \tag{7}$$

A description of the variables in these equations is shown in Table 1. The subscripts v and s indicate the vagal and sympathetic branches, respectively. The CBR uses the difference between the carotid blood pressure (P_{sa}) and its basal value (P_{san}) as the input. The LSR uses the excess of the pulmonary volume over the amount at the

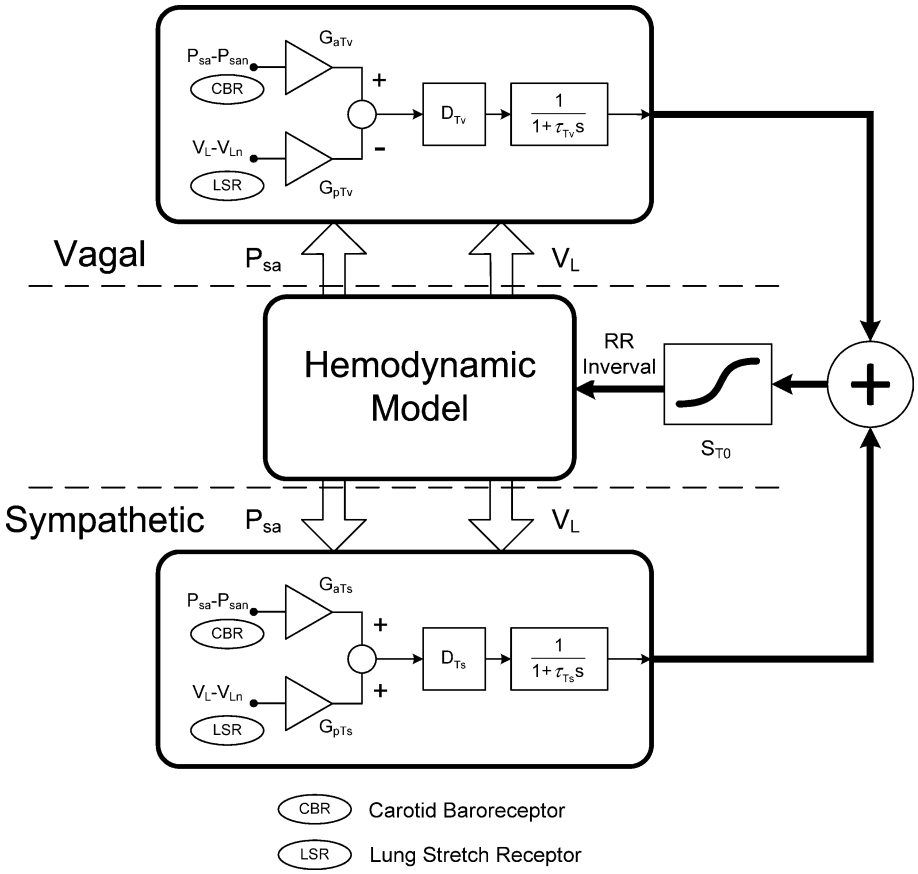

Fig. 1 Block diagram of the model of heart rate regulation. The variation of RR interval (RRI) is regulated by the co-activation of the sympathetic and vagal branches. Each branch takes the stimuli from the carotid baroreceptor (CBR) and the lung stretch receptor (LSR) as the inputs. The inputs are amplified, combined, delayed, and filtered. The outputs of the two branches are summed and processed by a sigmoidal function to generate the updated RRI. A description of the *symbols* in the block diagram is provided in Table 1

Table 1 Interpretations and the basal values of the parameters of the heart rate regulation model [44]

Parameter	Definition	Value	Units
G_{aTs}	Carotid baroreceptor gain on sympathetic control on heart period	0.015	mmHg^{-1}
G_{pTs}	Lung receptor gain on sympathetic control on heart period	0	L^{-1}
G_{aTv}	Carotid baroreceptor gain on vagal control on heart period	0.028	mmHg^{-1}
G_{pTv}	Lung receptor gain on vagal control on heart period	0.25	L^{-1}
D_{Ts}	Time delay of sympathetic control on heart period	3	s
D_{Tv}	Time delay of vagal control on heart period	0.5	s
τ_{Ts}	Time constant of sympathetic control on heart period	1.8	s
τ_{Tv}	Time constant of vagal control on heart period	0.8	s
P_{san}	Normal mean value of instantaneous systemic arterial pressure	95	mmHg
V_{Ln}	Lung volume at the end of expiration	2.3	L
$RR_{\min}$	Smallest heart period	0.558	s
$RR_{\max}$	Largest heart period	1.308	s
S_{T0}	Central slope for the sigmoidal function of heart period regulation	1	

end of expiration V_{Ln} as the input. The inputs are amplified (by multiplying with the sympathetic gains G_{aTs} and G_{pTs}, and the vagal gains G_{aTv} and G_{pTv}), combined, delayed (by D_{Ts} and D_{Tv}), and filtered by a low-pass system (with the time constants τ_{Ts} and τ_{Tv}) to generate the sympathetic and vagal stimuli (x_{Ts} and x_{Tv}). The stimuli are summed and processed by a sigmoidal system [Eq. (7)] to produce the RRI value RR, with S_{T0} as the slope of the sigmoidal curve, $RR_{\max}$ as the maximum RRI, and $RR_{\min}$ as the minimum RRI.

The parameters of the model were taken from previous reports [43, 44]. The parameters of the hemodynamic model were assigned to suit a person with 70 kg body weight [43]. The parameters of the regulating model were set according to human and dog experiments [44]. In particular, for the model of heart rate regulation, the gains of

each input (G_{aTs}, G_{pTs}, G_{aTv}, and G_{pTv}) were determined to conform to the variation of heart rate observed in young healthy men during pharmacological changes in arterial pressure [20]. The time delays (D_{Ts} and D_{Tv}) and time constants (τ_{Ts} and τ_{Tv}) were assigned following from the fact that vagal stimulation is completed within two or three beats, whereas the sympathetic stimulation on heart rate takes effect over a slower timescale, usually within a few seconds [44]. The parameters of the model of heart rate regulation are described in Table 1.

2.2 Multi-scale DC and AC calculation

The PRSA algorithm [5, 6] was applied to compute the multi-scale DCs and ACs from the RRI series produced by the model. Taking the DC calculation as an example, in brief, the first step of PRSA was to select the anchor points from the RRI series. The *i*th RRI was selected as the anchor point if the neighboring RRIs conformed to

$$\frac{1}{T}\sum_{k=0}^{T-1} \mathrm{RR}_{i+k} > \frac{1}{T}\sum_{k=1}^{T} \mathrm{RR}_{i-k}, \tag{8}$$

where T was the timescale that determined the number of points of the moving average low-pass filter for the anchor point selection. The sections with length $2L+1$ around the anchor points were determined, where L was the length of the slowest fluctuations in the signal. The determined sections were aligned according to the anchor points and averaged to create the PRSA average $\overline{\mathrm{RR}}$. DC was obtained as the wavelet coefficient of the PRSA average $\overline{\mathrm{RR}}$

$$\mathrm{DC} = \sum_{l=-L}^{L} \overline{\mathrm{RR}}_l \frac{h(l/s)}{s}, \tag{9}$$

where $h(t) = -1/2$ (for $-1 \le t < 0$), $+1/2$ (for $0 \le t < 1$), 0 (otherwise) was the Haar wavelet function, and s was the scale of the wavelet. The scale s determined the frequency components in the averaged RRI series that most influenced the values of DC and AC. Corresponding to a wavelet at scale s, the pseudo frequency F_s is approximated as [1]

$$F_s \approx \frac{F_c}{s \cdot \Delta t} \tag{10}$$

where F_c is the center frequency of a wavelet in Hz, and Δt is the sampling period. Following this relationship, the F_s for Haar wavelet can be obtained as [33]

$$F_s \approx \frac{0.371}{s \cdot \mathrm{RR}_{\mathrm{mean}}} \tag{11}$$

where $\mathrm{RR}_{\mathrm{mean}}$ is the mean RRI of the series. The calculation of AC proceeded in a similar fashion, except for the criterion of the anchor point selection, which describes the heart rate acceleration as

$$\frac{1}{T}\sum_{k=0}^{T-1} \mathrm{RR}_{i+k} < \frac{1}{T}\sum_{k=1}^{T} \mathrm{RR}_{i-k} \tag{12}$$

The DC and AC computed based on the timescale T and wavelet scale s were represented as DC(T,s) and AC(T,s). In particular, the conventional DC and AC, which correspond to $T = 1$ and $s = 2$ [5], were represented as $\mathrm{DC}_{\mathrm{conv}}$ and $\mathrm{AC}_{\mathrm{conv}}$, respectively.

2.3 Model validation and data analysis

The frequency spectral properties of HRV were analyzed to validate the model. Physiologically, there are mainly two characteristic frequency components in the HRV [40]. One is a LF component, which ranges from 0.04 to 0.15 Hz. The other is a HF component, which ranges from 0.15 to 0.4 Hz. The power spectral densities (PSDs) for the basal condition and for the conditions with ±20 % variations of the basal sympathetic and vagal gains were computed, and we examined whether the model was able to generate physiologically correct LF and HF peaks to confirm the model validity.

The model was simulated by a numerical program written in Matlab R2010b (MathWorks, Natick, MA, USA). Each simulation ran for 1200 s. The data of the last 1000 s were involved in the analysis. The step size of the simulation was set to 0.01 s. An RRI value was produced for each step. As a result, the generated RRI series could be treated as a resampled signal with a 100-Hz sampling frequency. Before further data analysis, the RRI series was preprocessed. For the PSD analysis, the signal was down-sampled to 4 Hz and detrended [39]. A Butterworth low-pass filter with a cutoff frequency of 0.4 Hz was applied to the signal before the down-sampling procedure to avoid aliasing. The Welch periodogram approach [2] was used to compute the PSD. The RRI series were further down-sampled to 1 Hz for the DC and AC calculations.

To determine the correlations of DC and AC to the ANS functions, the simulation ran for 400 times. For each run, the sympathetic and vagal gains were randomly selected from the range of ±20 % of their basal levels and remained unchanged during the simulation. Modification of the ANS activities was carried out by adjusting G_{aTs} and G_{pTs} for the sympathetic branch, and G_{aTv} and G_{pTv} for the vagal branch. In addition, the time delays, D_{Tv} and D_{Ts}, and the time constants, τ_{Tv} and τ_{Ts}, were randomized with ±20 % fluctuations of their basal values to ensure the generality of the analysis. Multi-scale DC(T,s) and AC(T,s) were calculated for each level of ANS activity. The segment length L was set to 60 [5]. The absolute DC and AC values were

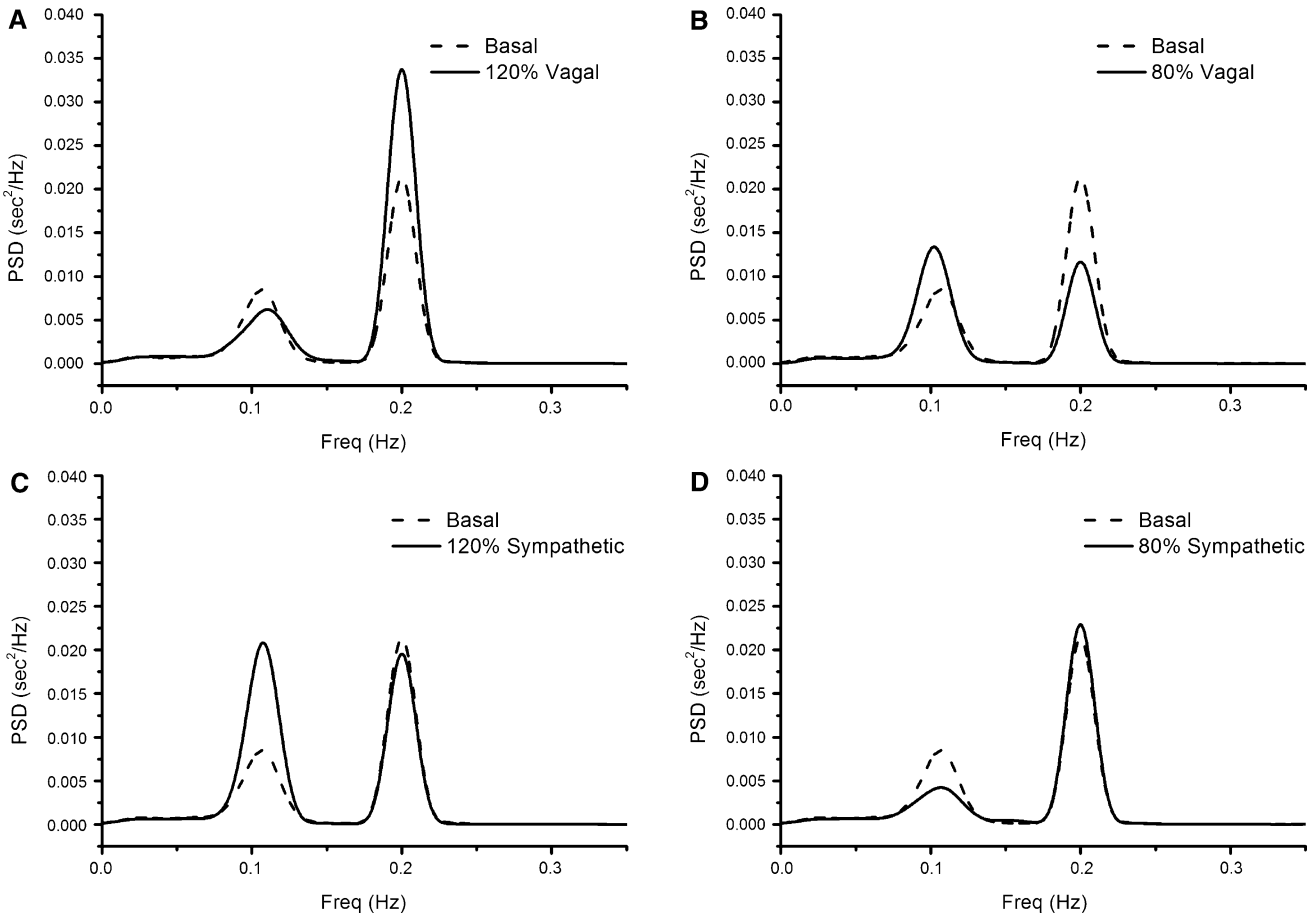

Fig. 2 PSDs of the RRI series under basal conditions and the states with modified sympathetic and vagal gains. The PSDs obtained by increasing (**a**) and decreasing (**b**) the vagal gains by 20 % and by increasing (**c**) and decreasing (**d**) the sympathetic gains by 20 % are plotted in *solid lines*. The PSD under the basal condition is plotted in the *dashed line* for comparison

used in the correlation analysis because they expressed the quantity of the extracted quasi-periodic components. Pearson's correlation analysis was used to evaluate the relationship between the indices and the ANS activities. $p < 0.001$ was considered statistically significant.

Sensitivity analysis was performed to verify the robustness of the correlation analysis with respect to the basal mean RRI and the response of the sinus node to the ANS stimulation. First, the basal mean RRI was modified via changing RR_{max} and RR_{min} simultaneously by ±20 %. Second, the response of the sinus node to the ANS stimulation S_{T0} was increased and decreased by 20 %, respectively. All statistical analysis was performed with SPSS version 19 (IBM, Armonk, NY, USA).

3 Results

The PSDs of the RRI series at the basal condition and at the conditions with ±20 % fluctuations of the ANS gains are plotted in Fig. 2. Increasing the vagal gains led to a significant increase in the HF component (Fig. 2a). The LF component was reduced despite the fact that the sympathetic gain was maintained. Opposite variations of LF and HF were also observed when the vagal gains were decreased (Fig. 2b). The adjustment in the LF was positively dependent upon the sympathetic gains (Fig. 2c, d). For example, increasing the sympathetic gains induced a significant increase in the LF power (Fig. 2c). By contrast, the HF component exhibited slight modification. These observations are in agreement with a human experiment that used autonomic blocking agents and postural changes [28] and were similar to the simulation results of Ursino et al. [44].

The PRSA averages at the basal condition and at the conditions with ±20 % fluctuations of the ANS gains are plotted in Fig. 3. The HF and LF oscillations are observed on the PRSA average curve. With the increase of the vagal gains, the HF oscillation was enhanced while the LF oscillation was damped (Fig. 3a, b). Opposite variations of the HF and LF oscillations were found when the vagal gains

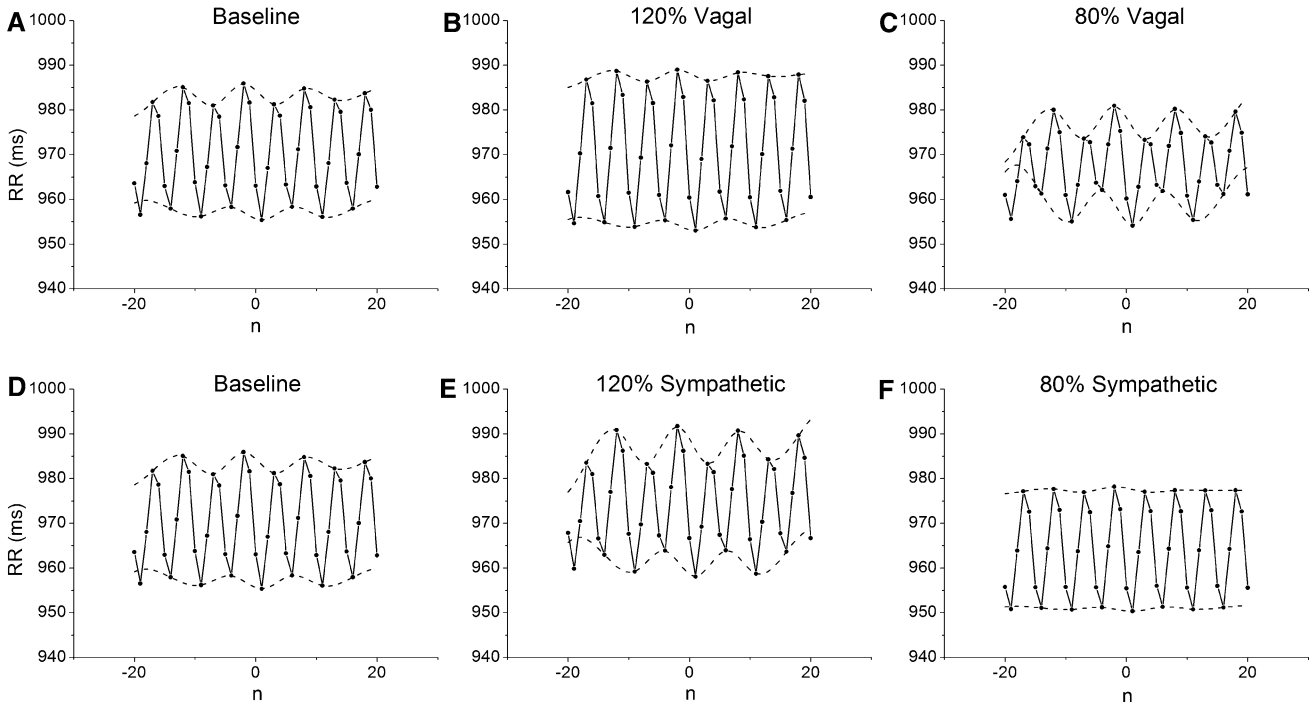

Fig. 3 The phase-rectified signal averaging (PRSA) curves at the basal condition (**a**, **d**) and at the conditions with (**b**) 120 % vagal gains, (**c**) 80 % vagal gains, (**e**) 120 % sympathetic gains, and (**f**) 80 % sympathetic gains. Oscillations are observed at two frequencies. One is the high-frequency oscillation, which has a cycle of 5–6 RRIs. The other is the low-frequency oscillation, which is indicated by the *envelope lines*

Table 2 Mean RR interval (RRI), DC_{conv}, and AC_{conv} at the basal condition and at the conditions with ±20 % fluctuations of the sympathetic and vagal gains

	Mean RRI (ms)	DC_{conv} (ms)	AC_{conv} (ms)
Baseline	970.65	14.53	−12.28
80 % Vagal	967.49	11.97	−10.49
120 % Vagal	971.41	19.09	−14.61
80 % Sympathetic	964.32	15.59	−11.39
120 % Sympathetic	974.51	14.84	−13.29

were decreased (Fig. 3a, c). The sympathetic gains are positively related to the LF oscillation (Fig. 3d–f). For example, when the sympathetic gains were increased by 20 %, the LF oscillation became larger while the HF oscillation remained at the basal level (Fig. 3d, e). The corresponding DC_{conv} and AC_{conv} obtained from the PRSA averages are given in Table 2. It is shown that both DC_{conv} and AC_{conv} were strongly influenced by the change of the vagal gains but slightly modified by the variation of the sympathetic gains.

The correlations of $|DC(T,s)|$ and $|AC(T,s)|$ to the sympathetic and vagal functions with both T and s from one to five are shown in Fig. 4. Under small timescales and wavelet scales, $|DC(T,s)|$ and $|AC(T,s)|$ were strongly correlated with vagal activity. Taking the conventional scales ($T = 1$, $s = 2$) as an example, both $|DC_{conv}|$ and $|AC_{conv}|$ showed significant positive correlation with vagal activity ($|DC_{conv}|$: $R = 0.67$, $p < 0.001$, Fig. 5a, $|AC_{conv}|$: $R = 0.39$, $p < 0.001$, Fig. 5b). Neither indices were correlated with sympathetic activity ($|DC_{conv}|$: $R = 0.04$, $p = 0.451$, Fig. 5c, $|AC_{conv}|$: $R = 0.08$, $p = 0.098$, Fig. 5d).

With increasing timescales and wavelet scales, the correlation of the indices to the vagal activity transited from positive to negative, whereas the correlation between the indices and the sympathetic activity was enhanced significantly (Fig. 4). The maximal sum of R^2 between the indices and the ANS functions appeared at $T = 3$ and $s = 5$. $|DC(3,5)|$ and $|AC(3,5)|$ showed significant negative correlation to vagal activity ($|DC(3,5)|$: $R = -0.35$, $p < 0.001$, Fig. 6a, $|AC(3,5)|$: $R = -0.34$, $p < 0.001$, Fig. 6b), and significant positive correlation to sympathetic activity ($|DC(3,5)|$: $R = 0.48$, $p < 0.001$, Fig. 6c, $|AC(3,5)|$: $R = 0.47$, $p < 0.001$, Fig. 6d).

The conclusion of the correlation analysis held in the sensitivity analysis. As shown in Fig. 7, with ±20 % fluctuations of the basal RRI and the response of the sinus node to ANS stimulation, $|DC_{conv}|$ and $|AC_{conv}|$ still show high positive correlation with the vagal gains and poor correlation with the sympathetic gains. $|DC(3,5)|$ and $|AC(3,5)|$ maintain their negative correlation with the vagal activities and positive correlation with the sympathetic activities.

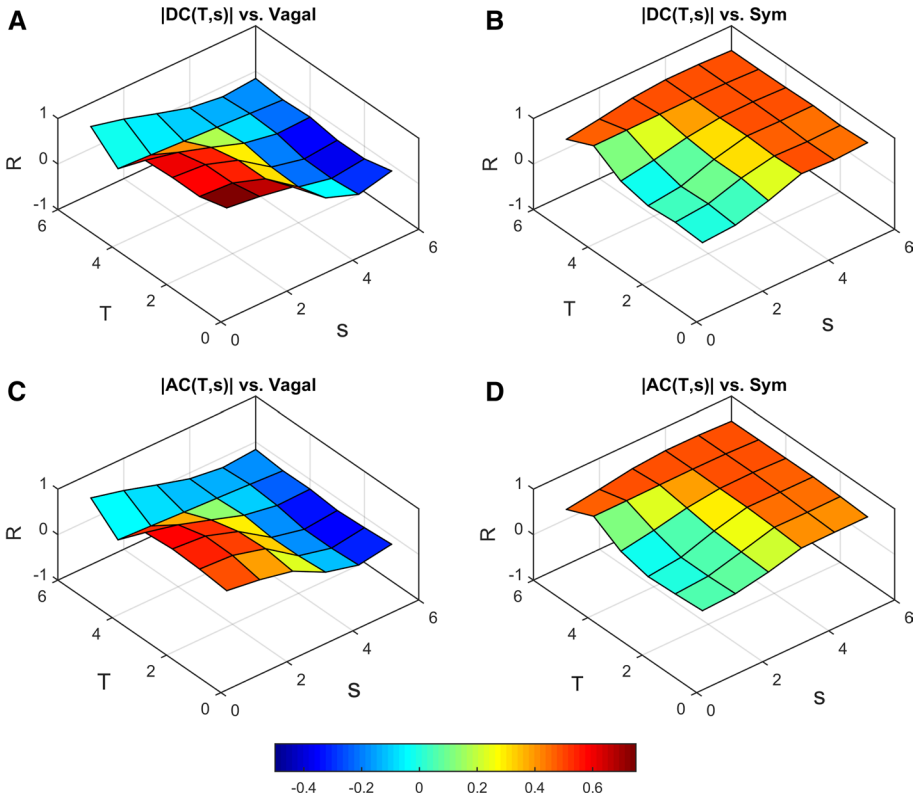

Fig. 4 The correlation coefficients of |DC(T,s)| to vagal activity (**a**) and sympathetic activity (**b**), and the correlation coefficients of |AC(T,s)| to vagal activity (**c**) and sympathetic activity (**d**). *R* correlation coefficient, *T* timescale, *s* wavelet scale. Both *T* and *s* range from one to five to include all the relevant frequencies in the simulated HRV

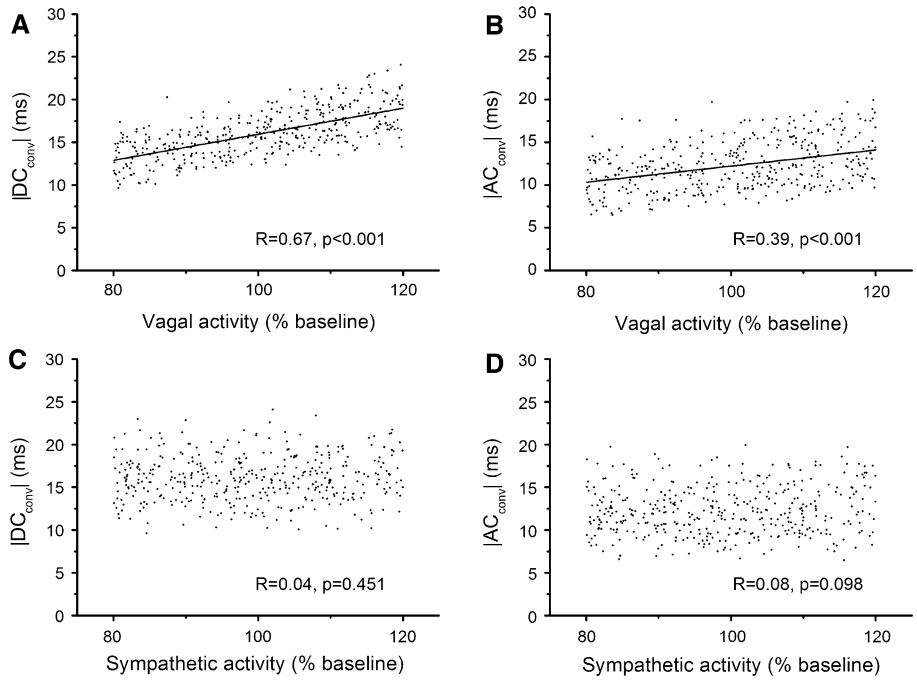

Fig. 5 The correlation of $|DC_{conv}|$ and $|AC_{conv}|$ to ANS activity. **a** $|DC_{conv}|$ versus vagal activity. **b** $|AC_{conv}|$ versus vagal activity. **c** $|DC_{conv}|$ versus sympathetic activity. **d** $|AC_{conv}|$ versus sympathetic activity. The *scattered dots* represent the $|DC_{conv}|$ and $|AC_{conv}|$ values calculated at the corresponding levels of ANS function. $|DC_{conv}|$ and $|AC_{conv}|$ were positively correlated with vagal activity, but uncorrelated with sympathetic activity

4 Discussion

4.1 Validity of the model for DC and AC analysis

As DC and AC are generally regarded as variants of the HRV index [22], our analysis of DC and AC using a cardiovascular model relied on correct simulation of HRV with respect to the ANS functions. The common physiological viewpoint [7, 40] suggests that the LF component is influenced by the interaction of the sympathetic and vagal activities. Excitation of sympathetic activity and/or blockage of vagal activity are expected to increase the LF power.

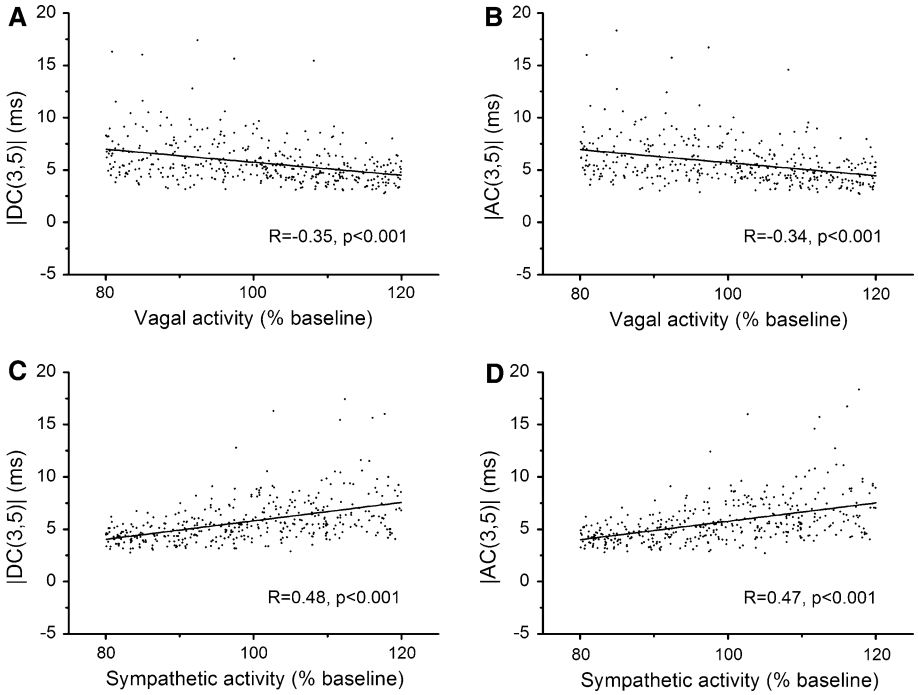

Fig. 6 The correlation of |DC(3,5)| and |AC(3,5)| to ANS activity. **a** |DC(3,5)| versus vagal activity. **b** |AC(3,5)| versus vagal activity. **c** |DC(3,5)| versus sympathetic activity. **d** |AC(3,5)| versus sympathetic activity. The *scattered dots* represent the |DC(3,5)| and |AC(3,5)| values calculated at the corresponding levels of ANS activity. |DC(3,5)| and |AC(3,5)| were positively correlated with sympathetic activity and negatively correlated with vagal activity

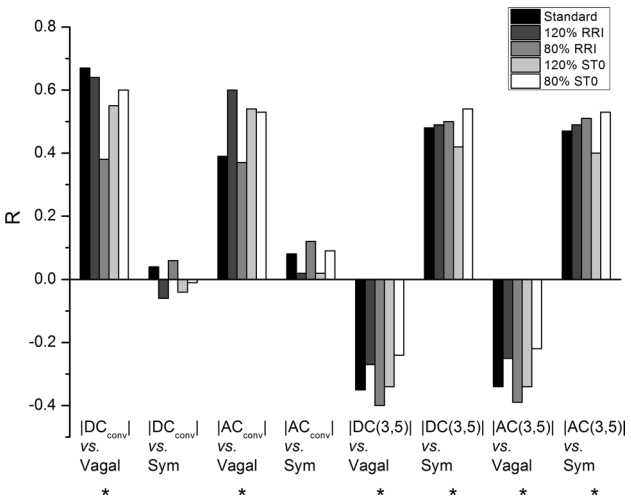

Fig. 7 Robustness of the correlation analysis. *Sym* sympathetic. The correlation analysis was tested under ±20 % variation of the basal RR interval, and ±20 % of the response of the sinus node to ANS stimulation, respectively, to test its robustness. $*p < 0.001$

Further, the HF component is positively related to vagal activity. The PSD analysis was consistent with these physiological viewpoints. Figure 2 shows that an elevation in the vagal gain led to an increased HF power and a decreased LF power, whereas an elevation in the sympathetic gain only led to an increased LF power. Reverse adjustment of the cardiac autonomic activities in the model resulted in opposite changes in the power of the characteristic frequency components.

Some studies have reported opposite findings to our simulation results. For example, Houle and Billman showed a reduction in the LF power in response to exercise, which are common interventions for increasing cardiac sympathetic activity [15]. Taylor et al. [41] also found a reduction in the LF power when the cardiac vagal modulation was blocked by atropine. These discrepancies can be explained as follows. While the PSD analysis only changes the sympathetic and vagal gains in the model, the real interventions that modify ANS activity change both the gains and the 'working point' of the model, such as basal heart rate and sensitivity of the sigmoidal relationship, owing to complex physiological processes [44]. This leads to variations of total power in HRV. As a result, a direct comparison between the experiments and the simulation by absolute LF and HF power is inappropriate. In such a circumstance, the LF/HF ratio index should be considered. For example, in spite of the reduction in the LF power, Houle and Billman reported an increase of LF/HF ratio from 0.59 to 1.04 after exercise [15], and Taylor et al. [41] reported an increase of LF/HF ratio from 0.63 to 0.98 using atropine. Our simulation succeeded in reproducing the rise of LF/HF ratio. By increasing the sympathetic gains to 120 % or reducing the vagal gains to 80 % of the basal level, the LF/HF ratio was lifted from 0.60 to 1.30 or to 1.47, respectively. It suggests that the model is capable of simulating the balance between the LF and HF in HRV.

The characteristic LF and HF oscillations in the simulated RRI series were well extracted by the PRSA method. As shown in Fig. 3, the HF oscillation with a cycle of 5–6

RRI was clearly observed on the PRSA curves. The LF oscillation lasted over a longer scale, as indicated by the envelope lines. With the variation of the ANS gains, the change of the LF and HF oscillation in time domain agreed with that in the PSD analysis, indicating that the PRSA method is capable of detecting the characteristic frequency components masked in the non-stationary signals. The validity of the PRSA method permits the use of the model for DC and AC analysis.

4.2 Impact of the anchor point selection on the interpretation of DC and AC

Previous studies have inferred that the criterion of anchor point selection may determine the physiological background of DC and AC [3, 5, 17] and that DC_{conv} expresses vagal activity as the vagal stimulation evokes heart rate deceleration. Following this theory, Bas et al. [3] deduced that AC_{conv} is related to sympathetic activity. By contrast, we found that both DC_{conv} and AC_{conv} were strongly correlated with vagal activity, but were largely unaffected by sympathetic activity (Fig. 5), suggesting that despite their opposite criteria for anchor point selection, they do not differ in their physiological background. Our simulation results support the assumption of Campana et al. [8] that both DC and AC are vagally dependent, but contradict the inference that AC_{conv} reflects sympathetic activity [3].

Our findings may be explained based on the principles of the PRSA algorithm. The PRSA aims to extract the quasi-periodicities from non-stationary signals. Averaging the signal segments eliminates noise, and thus extracts the appropriate intrinsic frequencies only if the segments are well synchronized in phase [6, 27]. In the non-stationary RRI series, the exact phase cannot easily be determined. An increasing or decreasing trend is thus adopted as the reference phase for quasi-synchronization. It is important to note that the anchor point selection only alters the quality of the averaged series, but imposes no effect on the relationship of the indices to the ANS. The step that influences the physiological interpretation of the indices is the calculation of the index from the averaged series. Because both DC_{conv} and AC_{conv} are derived as the coefficient of the Haar wavelet at scale two, and according to Eq. (11) are most sensitive to the frequency $f \approx 0.191$ Hz (taking $RR_{mean} \approx 0.97$ s at the basal condition, Table 2), they primarily detect the HF oscillations of HRV, which are predominated by vagal function [40]. In consequence, the deceleration- and acceleration-related indices reflect similar properties of the ANS function under the same scales.

Our results may provide a new explanation for the superior predictive ability of DC_{conv} compared to AC_{conv} in clinical trials [5]. While Kantelhardt et al. [17] suggest that this was owing to the assumption that DC_{conv} and AC_{conv} reflect different aspects of the ANS, we suggest that the stronger correlation of DC_{conv} to the vagal activity (Fig. 5) accounts for the difference in their predictive abilities. This implies that the process of anchor point selection for DC_{conv} results in better extraction of the HF oscillations from the RRI series. It could probably be explained by the phenomenon of heart rate asymmetry (HRA), the asymmetrical patterns of heart rate acceleration and deceleration. Porta Index (PI) [31] is a representative HRA index, which measures the percentage of negative ΔRR with respect to the total number of nonzero ΔRR. ΔRR is calculated as $RR(i+\tau) - RR(i)$, where i is the index of the RRI in the series and τ is the timescale. With $\tau = 1$, Porta et al. [30] reported that PI is larger than 50 %. Our simulation obtained a PI as 55.09 % for the basal condition. PI over 50 % indicates that the decelerating runs are steeper than the accelerating runs [30]. Because the PRSA method can better extract the periodic components from the non-stationary signal with steeper runs of RRI [25, 27], both the experimental and simulated HRA support that DC has a stronger association with the ANS activities and thus shows superior prognostic ability in comparison with AC.

4.3 Relevance of the scales of DC and AC to their physiological significance

DCs and ACs under various timescales and wavelet scales were found to be differently correlated with ANS function. While DC_{conv} and AC_{conv} were exclusively dependent upon vagal activity (Fig. 5), DC(3,5) and AC(3,5) were positively influenced by sympathetic activity and negatively related to vagal activity (Fig. 6). The distinct frequency components measured by DC and AC may explain these differences. As described in Sect. 4.2, DC_{conv} and AC_{conv} reflect the HF heart rate oscillations. The HF components of HRV are assumed to mainly reflect vagal modulation [40]. Thus, DC_{conv} and AC_{conv} are vagally dependent. According to Eq. (11), DC(3,5) and AC(3,5) are most sensitive to the frequency of 0.077 Hz, which lies in the frequency range of the LF of HRV. Because the LF component is thought to reflect both sympathetic and vagal influences, activation of sympathetic modulation and inhibition of vagal modulation will lead to an elevation in its power. As a result, DC(3,5) and AC(3,5) are positively correlated with the sympathetic function and negatively correlated with the vagal function.

Close degrees of correlation of DC(3,5) and AC(3,5) with the ANS activities are observed (Fig. 6). The absence of HRA at longer timescale may account for the phenomenon. With the elevation of τ, Porta et al. [30] reported a PI closer to 50 % in comparison with that obtained at $\tau = 1$. Our model achieved a PI as 49.94 % for the basal condition with $\tau = 3$. As a result, the rates of steepness of the decelerating and accelerating runs are similar at the longer

timescales, leading to close effects of the PRSA processing with deceleration- and acceleration-related anchor point selection, and thus similar degrees of correlation of the indices with the ANS activities.

Our results help to interpret the findings of Kisohara et al. [19], who reported that the multi-scale DCs and ACs for measuring long-term ($T = 2$, $s = 7$) heart rate dynamics show predictive abilities comparable to but also independent of that of DC_{conv} and AC_{conv}, suggesting that the multi-scale DCs and ACs reflect different aspects of HRV from the conventional indices. According to Eq. (11), the indices with $s = 7$ characterize the LF components. The strong and independent predictive ability of the LF power of HRV [11] supports the fact that DC(2,7) and AC(2,7) are independent of the conventional DC and AC in predicting SCD.

With respect to the various optimal values of T and s reported in recent multi-scale PRSA studies [12, 19, 33, 38], it is worth noting that the optimal timescales and wavelet scales depend on the average heart rate of the subjects. According to Eq. (10), the frequency-domain properties of the PRSA are influenced by both the scales and the average beat-to-beat time interval. Thus, it is imperative to provide indices with proper scales for subjects with different basal heart rates. Particular attention is required when applying the multi-scale PRSA method to detect fetal status as fetal heart rate is much higher than that in adults.

4.4 Limitations

The present model has some limitations which are worth discussing. First, the parameters of the ANS regulating model were partly derived from dog experiments. Ursino et al. [44] have made efforts to eliminate the barriers that prevent its application to human. The baroreflex gains in the model were determined based on both dog and human experiments. Initially, the preliminary sympathetic gains were obtained from vagotomized dog experiments. Then, the sympathetic and vagal gains were refined to fit the heart rate variation in human [20]. Ursino et al. [44] also suggested that the dynamic characteristics of the autonomic loops (time delays and time constants in the model) are significantly different among animal species. To account for this, we randomized the time delays and time constants in the simulation. By these efforts, the model succeeded in simulating the HRV properties in frequency domain, the DC and AC indices, as well as the phenomenon of HRA. Even so, it is better to set the model parameters based on human data to study specific human physiological problems.

Second, the factors involved in generating the characteristic frequency components were simplified [44]. The model only takes carotid baroreflex and lung stretch controls as the main regulators of HRV. The other potential mechanisms for HRV include central, humoral, and vasomotor factors, etc. As known, the respiratory sinus arrhythmia (RSA), characterized by rhythmical changes of the heart period at the respiratory rate, is not only influenced by the stretching of the lung receptors, but also highly regulated by the central respiratory stimulation. Neglecting the central mechanism, the model may be limited in simulating respiration regulated HRV properties. Although Fonoberova et al. [10] reported that the model produced results in agreement with the experiments under various controlled breathing rhythms, comprehensive models should be developed to investigate the separated contributions of the respiratory center and the lung stretching receptors.

Third, the standard DC and AC are based on 24-h Holter recordings [5]. However, the model only involves the short-term regulation of heart period governed by carotid baroreflex and the pulmonary stretch receptor, and is thus limited in producing the heart rate variation caused by long-term regulation, such as circadian rhythm. Although the short-term DC and AC are strong predictors of cardiovascular diseases [34], incorporating the long-term cardiac regulation into the model is necessary for future development of DC and AC analysis.

5 Conclusions

We studied the correlation of DC and AC to ANS activity using a cardiovascular system model, in which the states of the ANS could be adjusted quantitatively, and the RRI series under various ANS states could be generated for DC and AC computations. The multi-scale PRSA analysis suggested that the physiological relevance of DC and AC to the ANS is determined by the timescales and wavelet scales, but is not influenced by the criteria for anchor point selection. We also found that DC_{conv} and AC_{conv} were exclusively dependent upon the vagal activity, with DC superior to AC in sensitivity. By contrast, the DC(3,5) and AC(3,5) were positively correlated with sympathetic activity, but negatively correlated with vagal activity. This study clarified the correlations of DC and AC to the ANS from the perspective of computational physiology, and will promote the application of these indices in future clinical practice.

Acknowledgments This research was supported by the National Natural Science Foundation of China (Grant Nos. 81401491, 81271662), the Natural Science Foundation of Zhejiang Province (Grant No. LQ14H180001), and Zhejiang Provincial Key Laboratory of Communication Networks and Applications.

Compliance with ethical standards

Conflict of interest The authors declare that they have no conflict of interest.

References

1. Adeli H, Zhou Z, Dadmehr N (2003) Analysis of EEG records in an epileptic patient using wavelet transform. J Neurosci Methods 123:69–87
2. Akay M (1994) Biomedical signal processing. Academic, San Diego
3. Bas R, Vallverdú M, Valencia JF, Voss A, de Luna AB, Caminal P (2015) Evaluation of acceleration and deceleration cardiac processes using phase-rectified signal averaging in healthy and idiopathic dilated cardiomyopathy subjects. Med Eng Phys 37:195–202
4. Bauer A, Barthel P, Schneider R, Ulm K, Müller A, Joeinig A, Stich R, Kiviniemi A, Hnatkova K, Huikuri H, Schömig A, Malik M, Schmidt G (2009) Improved Stratification of Autonomic Regulation for risk prediction in post-infarction patients with preserved left ventricular function (ISAR-Risk). Eur Heart J 30:576–583
5. Bauer A, Kantelhardt JW, Barthel P, Schneider R, Makikallio T, Ulm K, Hnatkova K, Schornig A, Huikuri H, Bunde A, Malik M, Schmidt G (2006) Deceleration capacity of heart rate as a predictor of mortality after myocardial infarction: cohort study. Lancet 367:1674–1681
6. Bauer A, Kantelhardt JW, Bunde A, Barthel P, Schneider R, Malik M, Schmidt G (2006) Phase-rectified signal averaging detects quasi-periodicities in non-stationary data. Phys A 364:423–434
7. Billman GE (2011) Heart rate variability: a historical perspective. Front Physiol 2:1–13
8. Campana LM, Owens RL, Clifford GD, Pittman SD, Malhotra A (2010) Phase-rectified signal averaging as a sensitive index of autonomic changes with aging. J Appl Physiol 108:1668–1673
9. Chattipakorn N, Incharoen T, Kanlop N, Chattipakorn S (2007) Heart rate variability in myocardial infarction and heart failure. Int J Cardiol 120:289–296
10. Fonoberova M, Mezić I, Buckman JF, Fonoberov VA, Mezić A, Vaschillo EG, Mun E-Y, Vaschillo B, Bates ME (2014) A computational physiology approach to personalized treatment models: the beneficial effects of slow breathing on the human cardiovascular system. Am J Physiol Heart Circ Physiol 307:H1073–H1091
11. Galinier M, Pathak A, Fourcade J, Androdias C, Curnier D, Varnous S, Boveda S, Massabuau P, Fauvel M, Senard JM, Bounhoure JP (2000) Depressed low frequency power of heart rate variability as an independent predictor of sudden death in chronic heart failure. Eur Heart J 21:475–482
12. Georgieva A, Papageorghiou AT, Payne SJ, Moulden M, Redman CWG (2014) Phase-rectified signal averaging for intrapartum electronic fetal heart rate monitoring is related to acidaemia at birth. BJOG Int J Obstet Gy 121:889–894
13. Grassi G, Seravalle G, Cattaneo BM, Lanfranchi A, Vailati S, Giannattasio C, Del Bo A, Sala C, Bolla GB, Pozzi M (1995) Sympathetic activation and loss of reflex sympathetic control in mild congestive heart failure. Circulation 92:3206–3211
14. Guyenet PG (2006) The sympathetic control of blood pressure. Nat Rev Neurosci 7:335–346
15. Houle MS, Billman GE (1999) Low-frequency component of the heart rate variability spectrum: a poor marker of sympathetic activity. Am J Physiol Heart Circ Physiol 276:H215–H223
16. Huikuri HV, Perkiomaki JS, Maestri R, Pinna GD (2009) Clinical impact of evaluation of cardiovascular control by novel methods of heart rate dynamics. Philos Trans R Soc A 367:1223–1238
17. Kantelhardt JW, Bauer A, Schumann AY, Barthel P, Schneider R, Malik M, Schmidt G (2007) Phase-rectified signal averaging for the detection of quasi-periodicities and the prediction of cardiovascular risk. Chaos 17:015112
18. Kikuya M, Hozawa A, Ohokubo T, Tsuji I, Michimata M, Matsubara M, Ota M, Nagai K, Araki T, Satoh H, Ito S, Hisamichi S, Imai Y (2000) Prognostic significance of blood pressure and heart rate variabilities: the Ohasama study. Hypertension 36:901–906
19. Kisohara M, Stein PK, Yoshida Y, Suzuki M, Iizuka N, Carney RM, Watkins LL, Freedland KE, Blumenthal JA, Hayano J (2013) Multi-scale heart rate dynamics detected by phase-rectified signal averaging predicts mortality after acute myocardial infarction. Europace 15:437–443
20. Korner PI, West MJ, Shaw J, Uther JB (1974) 'Steady-state' properties of the baroreceptor-heart rate reflex in essential hypertension in man. Clin Exp Pharmacol Physiol 1:65–76
21. La Rovere MT, Pinna GD, Maestri R, Mortara A, Capomolla S, Febo O, Ferrari R, Franchini M, Gnemmi M, Opasich C, Riccardi PG, Traversi E, Cobelli F (2003) Short-term heart rate variability strongly predicts sudden cardiac death in chronic heart failure patients. Circulation 107:565–570
22. Lewek J, Wranicz JK, Guzik P, Chudzik M, Ruta J, Cygankiewicz I (2009) Clinical and electrocardiographic covariates of deceleration capacity in patients with ST-segment elevation myocardial infarction. Cardiol J 16:528–534
23. Lombardi F, Malliani A, Pagani M, Cerutti S (1996) Heart rate variability and its sympatho-vagal modulation. Cardiovasc Res 32:208–216
24. Mateo J, Laguna P (2003) Analysis of heart rate variability in the presence of ectopic beats using the heart timing signal. IEEE Trans Biomed Eng 50:334–343
25. Nasario O, Benchimol-Barbosa PR, Nadal J (2014) Refining the deceleration capacity index in phase-rectified signal averaging to assess physical conditioning level. J Electrocardiol 47:306–310
26. Olshansky B, Sabbah HN, Hauptman PJ, Colucci WS (2008) Parasympathetic nervous system and heart failure: pathophysiology and potential implications for therapy. Circulation 118:863–871
27. Pan Q, Gong Y, Gong S, Hu Q, Zhang Z, Yan J, Ning G (2010) Enhancing the deceleration capacity index of heart rate by modified-phase-rectified signal averaging. Med Biol Eng Comput 48:399–405
28. Pomeranz B, Macaulay RJ, Caudill MA, Kutz I, Adam D, Gordon D, Kilborn KM, Barger AC, Shannon DC, Cohen RJ et al (1985) Assessment of autonomic function in humans by heart rate spectral analysis. Am J Physiol Heart Circ Physiol 248:H151–H153
29. Ponikowski P, Anker SD, Chua TP, Szelemej R, Piepoli M, Adamopoulos S, Webb-Peploe MK, Harrington MD, Banasiak W, Wrabec K, Coats AJS (1997) Depressed heart rate variability as an independent predictor of death in chronic congestive heart failure secondary to ischemic or idiopathic dilated cardiomyopathy. Am J Cardiol 79:1645–1650
30. Porta A, Casali KR, Casali AG, Gnecchi-Ruscone T, Tobaldini E, Montano N, Lange S, Geue D, Cysarz D, Van Leeuwen P (2008) Temporal asymmetries of short-term heart period variability are linked to autonomic regulation. Am J Physiol Regul Integr Comp Physiol 295:R550–R557
31. Porta A, Guzzetti S, Montano N, Gnecchi-Ruscone T, Furlan R, Malliani A (2006) Time reversibility in short-term heart period variability. Comput Cardiol 2006:77–80
32. Ricca-Mallada R, Migliaro ER, Piskorski J, Guzik P (2012) Exercise training slows down heart rate and improves deceleration and acceleration capacity in patients with heart failure. J Electrocardiol 45:214–219
33. Rivolta MW, Stampalija T, Casati D, Richardson BS, Ross MG, Frasch MG, Bauer A, Ferrazzi E, Sassi R (2014) Acceleration and deceleration capacity of fetal heart rate in an in-vivo sheep model. PLoS ONE 9:e104193

34. Sacha J, Sobon J, Sacha K, Muller A, Schmidt G (2011) Short-term deceleration capacity reveals higher reproducibility than spectral heart rate variability indices during self-monitoring at home. Int J Cardiol 152:271–272
35. Schroeder EB, Chambless LE, Liao D, Prineas RJ, Evans GW, Rosamond WD, Heiss G (2005) Diabetes, glucose, insulin, and heart rate variability: the Atherosclerosis Risk in Communities (ARIC) study. Diabetes Care 28:668–674
36. Schroeder EB, Liao D, Chambless LE, Prineas RJ, Evans GW, Heiss G (2003) Hypertension, blood pressure, and heart rate variability: the Atherosclerosis Risk in Communities (ARIC) study. Hypertension 42:1106–1111
37. Singh N, Mironov D, Armstrong PW, Ross AM, Langer A, Investigators ftGES (1996) Heart rate variability assessment early after acute myocardial infarction: pathophysiological and prognostic correlates. Circulation 93:1388–1395
38. Stampalija T, Casati D, Montico M, Sassi R, Rivolta MW, Maggi V, Bauer A, Ferrazzi E (2015) Parameters influence on acceleration and deceleration capacity based on trans-abdominal ECG in early fetal growth restriction at different gestational age epochs. Eur J Obstet Gynecol Reprod Biol 188:104–112
39. Tarvainen MP, Ranta-aho PO, Karjalainen PA (2002) An advanced detrending method with application to HRV analysis. IEEE Trans Biomed Eng 49:172–175
40. Task Force of The European Society of Cardiology and The North American Society of Pacing and Electrophysiology (1996) Heart rate variability: standards of measurement, physiological interpretation, and clinical use. Circulation 93:1043–1065
41. Taylor JA, Carr DL, Myers CW, Eckberg DL (1998) Mechanisms underlying very-low-frequency RR-interval oscillations in humans. Circulation 98:547–555
42. Tsuji H, Larson MG, Venditti FJ, Manders ES, Evans JC, Feldman CL, Levy D (1996) impact of reduced heart rate variability on risk for cardiac events: the Framingham Heart study. Circulation 94:2850–2855
43. Ursino M (1998) Interaction between carotid baroregulation and the pulsating heart: a mathematical model. Am J Physiol Heart Circ Physiol 44:H1733–H1747
44. Ursino M, Magosso E (2003) Role of short-term cardiovascular regulation in heart period variability: a modeling study. Am J Physiol Heart Circ Physiol 284:H1479–H1493
45. Webb SW, Adgey AAJ, Pantridge JF (1972) Autonomic disturbance at onset of acute myocardial-infarction. Br Med J 3:89–92

Qing Pan received his Ph.D. degree from Dept. of Biomedical Engineering, Zhejiang University, China. He is a lecturer in Zhejiang University of Technology, China.

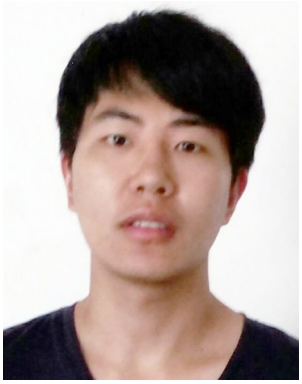

Gongzhan Zhou is a master student in the College of Information Engineering, Zhejiang University of Technology, China.

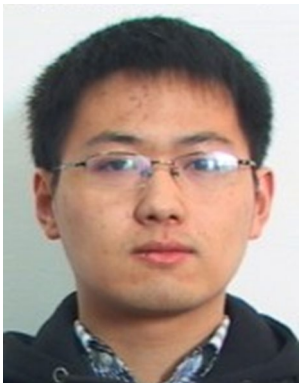

Ruofan Wang is a Ph.D. student in the Dept. of Biomedical Engineering, Zhejiang University, China.

Guolong Cai received his master degree from Dept. of Cardiology, Zhejiang University, China. He is a physician in the Dept. of ICU, Zhejiang Hospital, China.

Jing Yan received his master degree from Dept. of Cardiology, Zhejiang University, China. He is the dean of Zhejiang Hospital, China.

Luping Fang received his master degree from Dept. of Biomedical Engineering, Zhejiang University, China. He is a professor in Zhejiang University of Technology, China.

Gangmin Ning received his Ph.D. degree from Dept. of Biomedical Engineering, TU Ilmenau, Germany. He is a professor in the Dept. of Biomedical Engineering, Zhejiang University, China.